Journal of Solar Energy Research (JSER)

Journal homepage: jser.ut.ac.ir

Optimization of the Smart Grids Connected using an Improved P&O MPPT Algorithm and Parallel Active Filters

Kitmo[a*], Guy Bertrand Tchaya[a], Dieudonné Kaoga Kidmo[a*], Sadam Alphonse[b], Noël Djongyang[a]

[a]*Department of Renewable Energy, National Advanced School of Engineering, University of Maroua, P.O. Box 46 Maroua, Cameroon*
[b]*UFD PAI, Laboratory of analysis of simulation and testing, IUT of Ngaoundéré, P.O.Box 455, Ngaoundere, Cameroon.*
Received: 02-04-2021
Accepted: 10-08-2021

Abstract

This work describes a photovoltaic generator connected to the grid by associating the parallel active filters to improve the energy quality. The extraction of maximum power produced by the photovoltaic generators is done using the command of Maximum Power Point Tracking (MPPT) by modified perturb and observe (P&O) algorithm. Furthermore, to reduce the distortions due to the injected continuous quantities, the filtering of the harmonic quantities is done by four levels of active filters using three switching cells per arm connected downstream of the seven-level inverters. The proposed algorithm and the model of the active filter are evaluated. The calculation of the total harmonic distortion of the current after filtering shows acceptable results. The rate of 0.21% obtained proves the power factor correction. Finally, the simulation results show that this rate is in accordance with the Utility Connection Regulations. Besides, the performance of the algorithm has been demonstrated when the solar panels are subjected to variations in irradiance.

Keywords: Harmonics, P&O MPPT, Smart Grids, Filter.

1. Introduction

Nowadays, the demand and energy issues related to the quality of distribution and transmission of electrical energy are increasing, especially in the development of power electronic devices [1] . These parameters of electrical energy shaping must be considered before its use or connection to another source [2]. In the literature several filtering methods exist [3]. It is proposed in this work, the use of parallel active filters for energy compensation[4]. In the literature, several filtering methods exist [5]. This work proposes the use of parallel active filters for energy compensation [6]. The principle of compensation consists in injecting a current in phase opposition with the harmonics of the load (disturbance currents). The role of the active power filter is therefore to improve the quality of the electrical energy and to better respond to harmonic distortion problems [6]. These active filters, used in this work are based on multicellular inverters. They allow the suppression of harmonics and make the power factor close to unity [7]. Similarly, they reduce the inverse voltages injected into a source. They also reduces the reverse voltages applied to the filter switches [8]. One of the advantages of the multilevel inverter topology used in this work is to limit the reverse voltage stress on the switches. This is because the DC voltage of the boost converter bus is only a portion [9]. The MPPT (Maximum Power Point Tracking) control is used for its simplicity of implementation, the solar photovoltaic energy is a form of renewable energy. This energy allows producing electricity by transforming part of the solar radiation thanks to a solar cell. Photovoltaic installations are divided into two categories, depending on whether they operate in a non-autonomous manner or are connected to a public power distribution network.

* Corresponding authors:
E-mail address: kitmobahn@gmail.com (Kitmo)

In this study, the focus is on grid-connected installations. The need for the connection of photovoltaic generators results from the fact that the output power of the photovoltaic generator alone is not sufficient to meet the demand of the users. Therefore, it is necessary to connect these generators to the electrical networks.

In the first part of this work, the boost converter is presented as well as its system controlled by the MPPT [11]. The second part of this work is reserved for the modeling and control of seven-level inverters. The principle of the active filter and the structure of the three-phase inverter are studied in this part. The principle of the active filter and the structure of the three-phase inverter is studied in this part. The principle of the transformation of two voltage levels and three voltage levels, called two-phase Park transformation into three-phase, is also presented[12]. The reference currents and voltages are studied as well as the control of the multilevel inverter. The third part presents the results of the simulations made in MATLAB. And finally, a conclusion and perspectives constitute the last part of the article. In addition, the results of the discussion are largely analyzed and interpreted.

Nomenclature

n	Odd number
Va,b,c	Supply voltages
h_1	Fundamental of the output voltage.
$\propto_i$	Switching angles
S_i	Sign of cos
G	Illuminance (W / m^2)
C1,2	Capacitors boost converter (F)
D	Duty cycle of the boost converter
Ve	Input converter voltage (V)
Vs	Output converter current (A)
$\tilde{P}$	Instantaneous active power(w)
$\tilde{Q}$	Instantaneous Reactive power
Θ	Reference angle (rad)
P	Active power (W)
Q	Reactive power (VAR)
T	Temperature of the PV cell (° K),
I	Output current of the cell (A)
Iph	Photo-generated current (A)
A	Identity factor,
k	Boltzmann constant (13805-10-23 Nm/°K)
q	Electron charge (1.6-10-19 C),
Rs	Series resistance of the PV cell (Ω)
V	Operating Voltage (V)
V_T	Thermal Voltage (V)
N*p*	Number of cells in parallel
Io	Saturation current of the diode (A)
R*s*	Series Resistance of Cell (Ω)
N*s*	Number of cells in series
R*sh*	Shunt Resistance of Cell (Ω)
$I_{ref1,2,3}$	Reference grid voltages of three phases

2. Materials and Methods

2.1. Materials

2.1.1. Boost Chopper

The boost chopper is a static converter that converts DC energy into DC energy, and its duty cycle is controlled by the MPPT controller. The electrical diagram of this converter is presented in figure 1 and by [8] [13]. The role of the boost converter presented is to raise the voltage level delivered by the photovoltaic generator at its output. There are several types of DC-DC converters, including the boost chopper. For example, there is the double boost chopper which has more switches compared to the single boost. The latter can produce more switching losses, Joule effect losses, switching delay, even complexity of the MPPT algorithm, and risk of redundancy. It has been shown that the Joule effect increases when the voltage level or the filter switching cell increases. Because, each switch produces a voltage drop, according to the Joule law.

The boost converter is called a step-up converter. The input voltage Ve and output voltage Vs are of the same order of magnitude(α is the duty cycle of the boost converter), it is defined as follows[14]:

$$V_s = \frac{V_e}{1-\alpha} \qquad (1)$$

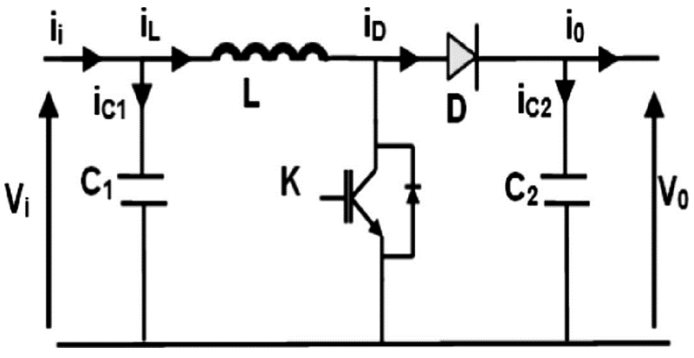

Fig. 1. Model of the Boost converter.

2.1.2. Diagram of the PV System

Fig. 2 shows the parts of the interface of the overall scheme, it consists of the photovoltaic generator, the boost converter, whose duty cycle is controlled by the PI controller.

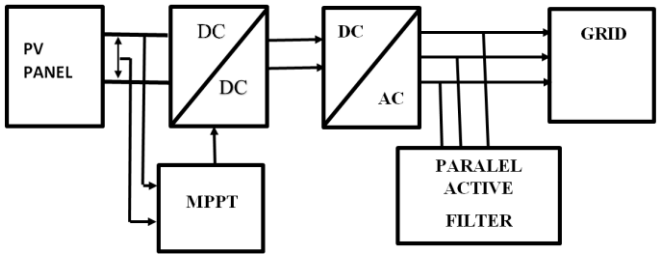

Fig. 2. PV system overview diagram.

2.1.3. Diagram of the four-Level Multicellular Filter

The active filters used are based on multicellular inverter. Fig. 3 illustrates the four-level which is used for the control of harmonics. This multicellular inverter is used as a parallel active filter. The active multicell filtering in this work is not only oriented towards the possibility of having data acquisition from integrated circuits and microcontrollers (Arduino, Raspberry) on the one hand. Thus, the active four-level filter with three switching cells per arm is chosen to allow the switches to support only a fraction of the voltage at their input by the PI regulation used for their control. On the other hand, the choice of this filter, which has fewer switches, is intended to reduce any kind of losses.

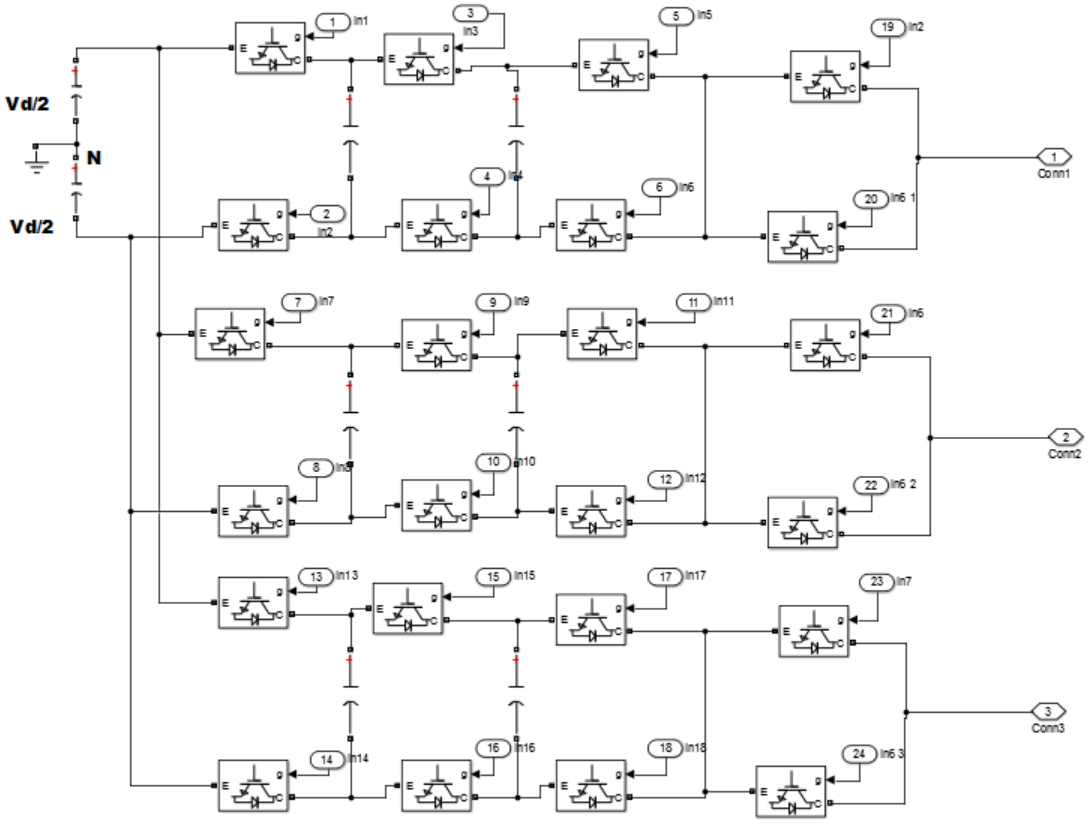

Fig. 3. Electrical model of the 4-level multicellular filter.

2.2. Methods

2.2.1. Maximum point method

The Maximum power Point tracking algorithm is an optimization technique which is used to extract the maximum power generated by a given signal [15]. An improved model based on this technique is presented in this works. It differs from the classical algorithm in that, it is based on a modified P&O algorithm. The flowchart of this MPPT algorithm is given in Fig. 4, it is clearly known that, it differs from the classical algorithms. This new algorithm is used to extract the maximum energy produced by the photovoltaic generator. In the literature, many algorithms are developed. P&O is considered as the most classical algorithm used, there are optimization algorithms such as the IC and Fuzzy-PI that M Sarvi,et al, compared as the solution for increasing the PV output voltage, the hybrid PSO and P&O algorithm that MH Zafar et al. proposed for Fast Altering illumination. The choice of an algorithm usually depends on the complexity of the problem to be solved. The P&O presented in this work is an improved and simplified version algorithm, it takes as parameters, the PV current and voltage input. In addition, its

flowchart in Fig. 4 is quite different from others.

Oscillations are made around the MPP, the small amplitude or step size variation will minimize the oscillation but will result in a slightly slow MPPT. Therefore, a variable step size will be used instead of fixed step size. In addition, the voltage perturbation is chosen to be proportional to the abrupt change in module power.

To increase the tracking speed and to solve the failure of the MPPT under rapid changes of irradiance, it is important to make an improvement. Knowing that the open-circuit voltage Voc is affected by the variation of irradiance and temperature, the reference voltage is set to a fraction of the open-circuit voltage to periodically check the variation of solar irradiance and to compensate for this variation, as follows:

$$V_{\text{ref}}^{*} = V_{\text{ref}} + C * \frac{\Delta P}{\Delta V} \qquad (2)$$

where *V*ref is the reference voltage of the MPP system; *C* is a PV constant that depends on manufacturer parameter.

$$V_{\text{ref}} = K_{\text{oc}} * V_{\text{oc}} \qquad (3)$$

where *K*oc is the proportionality constant for open-circuit voltage and ranges between 0.71 and 0.78 in this case.

$$\Delta V = V(k) - V(k-1) < \Delta V_{\text{SET}} \qquad (4)$$

$$I = \frac{I(k) - I(k-1)}{I(k-1)} < \Delta I_{\text{SET}} = \frac{I(k)}{N_P} \qquad (5)$$

where *k* is the sampling number; *NP* and *Ns* are the numbers of parallel and series modules in array, respectively; Δ*V*SET is the step size of voltage (v).

$$V_{\text{ref}} = V_{\text{PSC}}^{*} = \frac{N_{\text{sM}} \times V_{\text{ocM}}}{N_{\text{PM}} \times I_{\text{scM}}} \times I(k) \qquad (7)$$

where *V*∗PSC is the reference voltage of the MPP under partial shading (PSC) in volt; *V*ocM is the module open-circuit voltage in volt(v); *I*scM is the module short-circuit current in amp

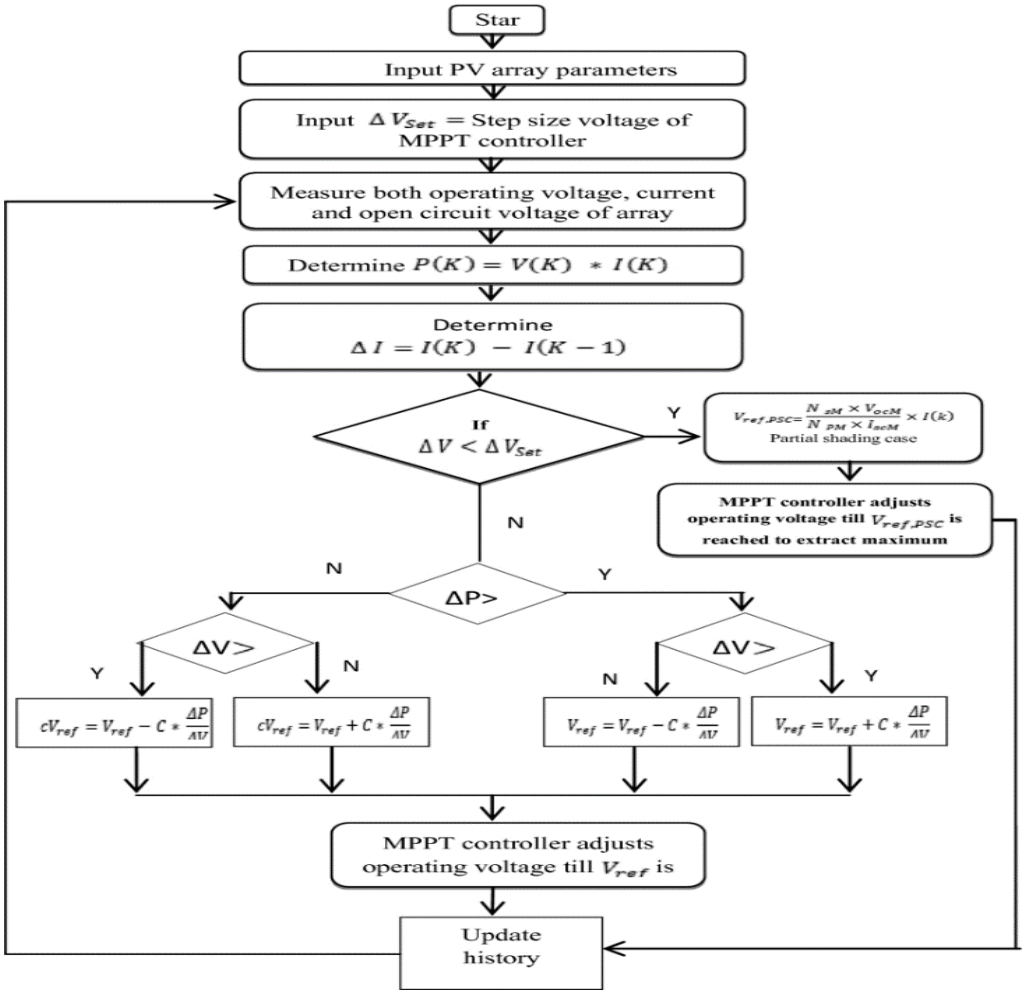

Fig. 4. Flowchart of the improved Perturb and Observe Algorithm.

2.2.2. The P&O Control Algorithm

This technique allows the current generated by the photovoltaic generators to maintain the upper extremum. Fig. 4. Shows the improved algorithm flowchart.

2.2.3. Equation of the generated Current

The equation for a mixed array formed by the series connection of Ns cells and Np parallel module is generalized as follows [16] :

$$I = N_p I_{ph} - N_p I_0 \left[exp\left(\frac{q\left(N_s V + \frac{N_s}{N_p} R_s I\right)}{N_s n K T} \right) - 1 \right] - \frac{q\left(N_s V + \frac{N_s}{N_p} R_s I\right)}{\frac{N_s}{N_p} R_{sh}} \quad (8)$$

Where:

I	:	Cell Output Current (A)
V	:	Operating Voltage (V).
V_T	:	Thermal Voltage (V).
N_P	:	Number of cells in parallel
I_{PH}	:	Photocurrent (A)
I_o	:	Saturation current of the diode (A)
R_S	:	Series Resistance of Cell (Ω)
N_S	:	Number of cells in series
R_{SH}	:	Shunt Resistance of Cell (Ω)
n	:	Ideality Factor
k		Boltzmann constant (13805-10-23 Nm/°K)

The irradiation is a random quantity [17], that is to say non-linear, But the boost chopper has an advantage due to its simplicity and its reduced number of switches [18]. It can improve the quality of the electrical quantities produced by the photovoltaic generators (PVG), when its duty cycle is defined in the best conditions.

2.2.4. The influence of temperature on the I-V characteristics and P-V curves of the PV module

The simulations are done for constant irradiance (G = 1000W / m^2) for different temperatures (20°C, 25°C, 30°C, 35°C, 40°C). Fig. 5 shows the I-V characteristics of PV module for different operating temperatures. The maximum power point is reached and remains constant during these variations.

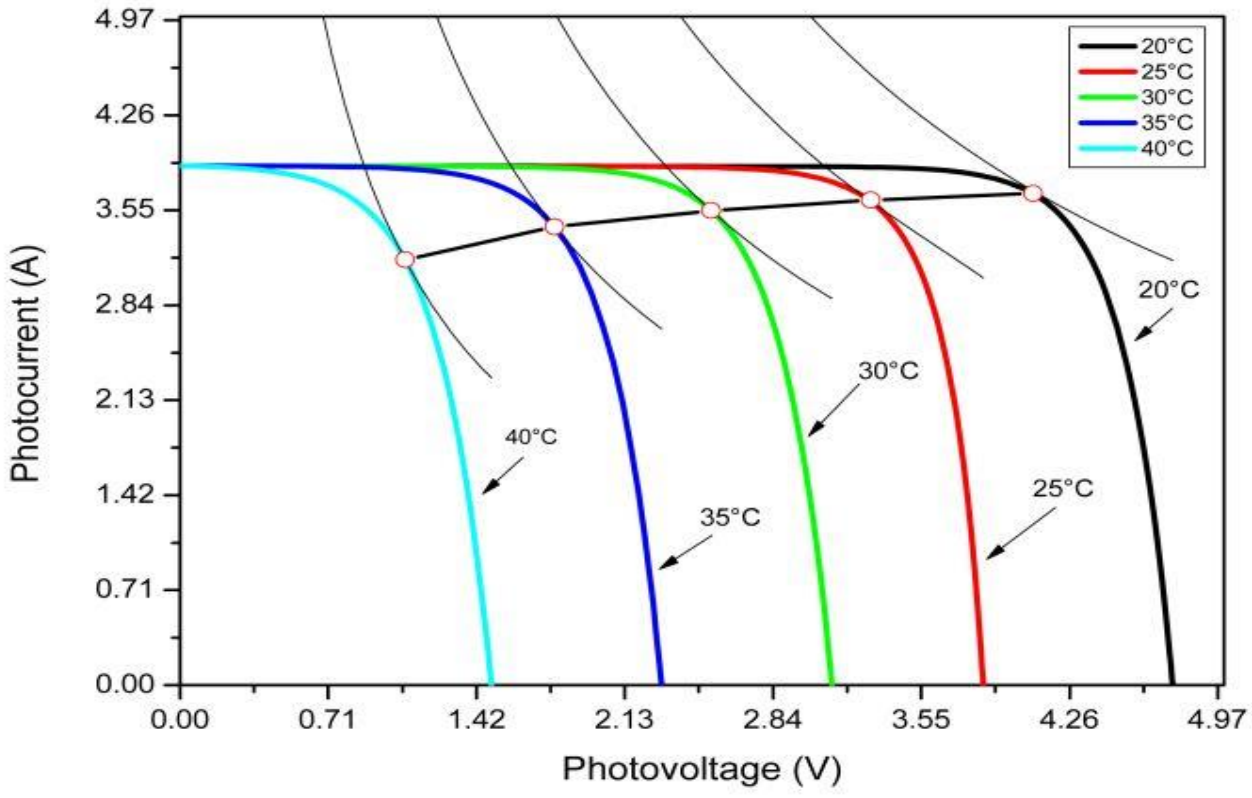

Fig. 5. impact of the temperature on the characteristic I-V and maximum power in the module

Fig. 6 shows the P-V curves for different variations of the Temperature of the photovoltaic module at a constant irradiance, known as test conditions (G = 1000W / m^2). The power point function is defined.

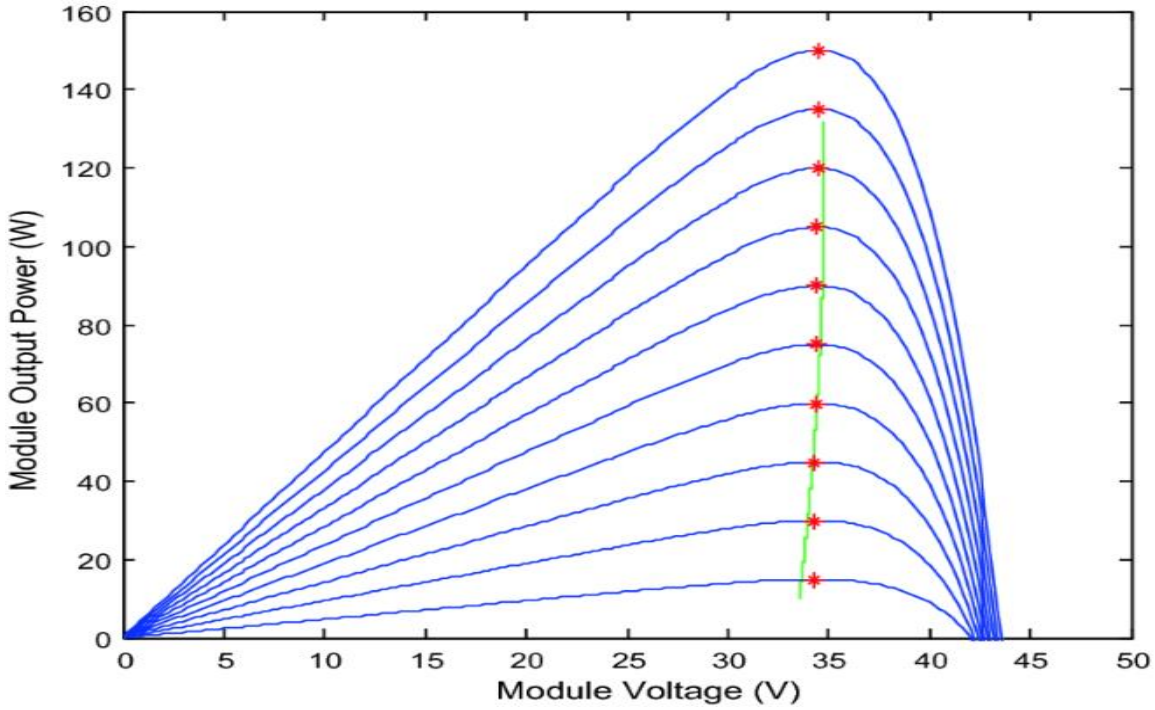

Fig. 6. impact of the temperature on the characteristic P-V Curves

2.2.5. Solar Module MSX 60/MSX 64 Characteristics

Table 2 provides the photovoltaic parameter of MSX 60/MSX 64 solar cell.

Table 1. Electrical Characteristics of the MSX 60/MSX 64 PV Module [19].

characteristics	reference		values
E *(G = 1000W / m²).*			1000
Maximum power(W)	P_m		15.80
Maximum voltage(V)	V_{mp}		18
Maximum current(mA/Cm²)	I_{mp}		47
Open circuit voltage(V)	V_{oc}		7.61
Open circuit current(mA/Cm²)	I_{scr}		43.8
Temperature range(°C)			-40° to +85
Number of cells in series	N_s		82
Number of cells in parallel	N_p		6

2.2.6. Seven-level inverter topology

The Fig. 7 illustrates seven-level inverters with cascade topology. These inverters offer the advantages of having several sources in parallel as well as having a reduced number of switches that. Many switches connected produce Joule effect losses [20].

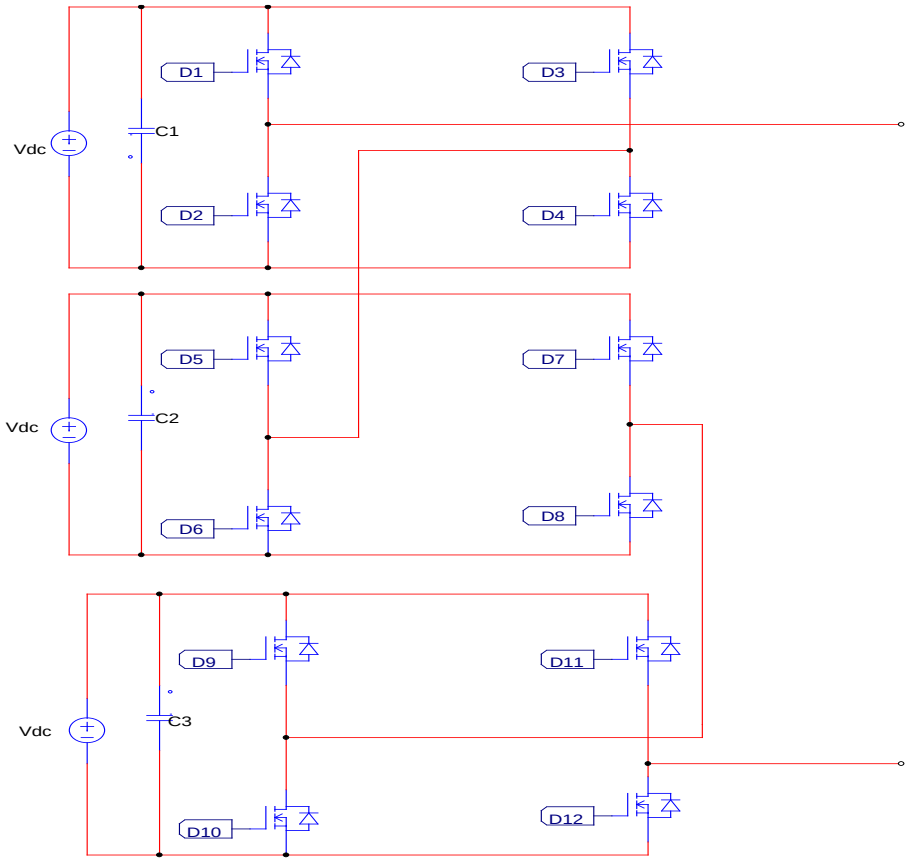

Fig. 7. The Control unit for complementary arms.

2.2.7. Triangular Sine PWM Modulation Technics

The Sine-triangular modulation consists of using triangular carriers of the same amplitude for a given level. Fig. 8 shows the modulation of a seven-level inverter with 6 carriers

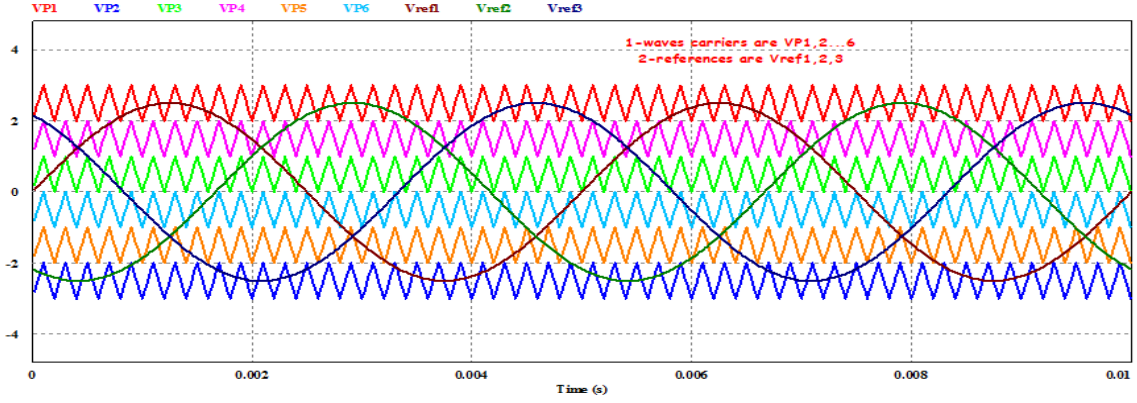

Fig. 8. Modulation of a seven-level inverter

The modulation of multilevel inverters are discussed , and the most used in the literature is that known as triangulo-sinusoidal [21] where the arms of each switching cell are complementary to each other two by two. Fig. 9 represents this switching cell.

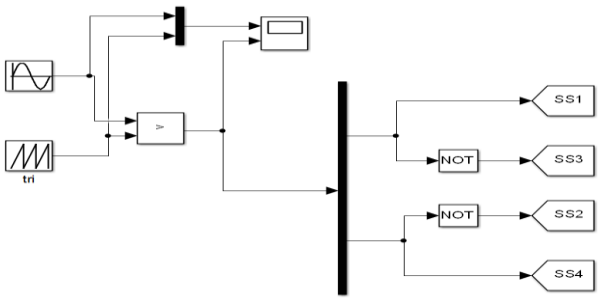

Fig. 9. Control unit for complementary arms.

2.2.8. The 7-level inverter output voltages before filtering

The simulation gave the shape of the voltage of a phase, which is represented in Fig. 10. This voltage between phase and neutral has a distorted form and this is due to the DC values produced by the photovoltaic generators (PVG).

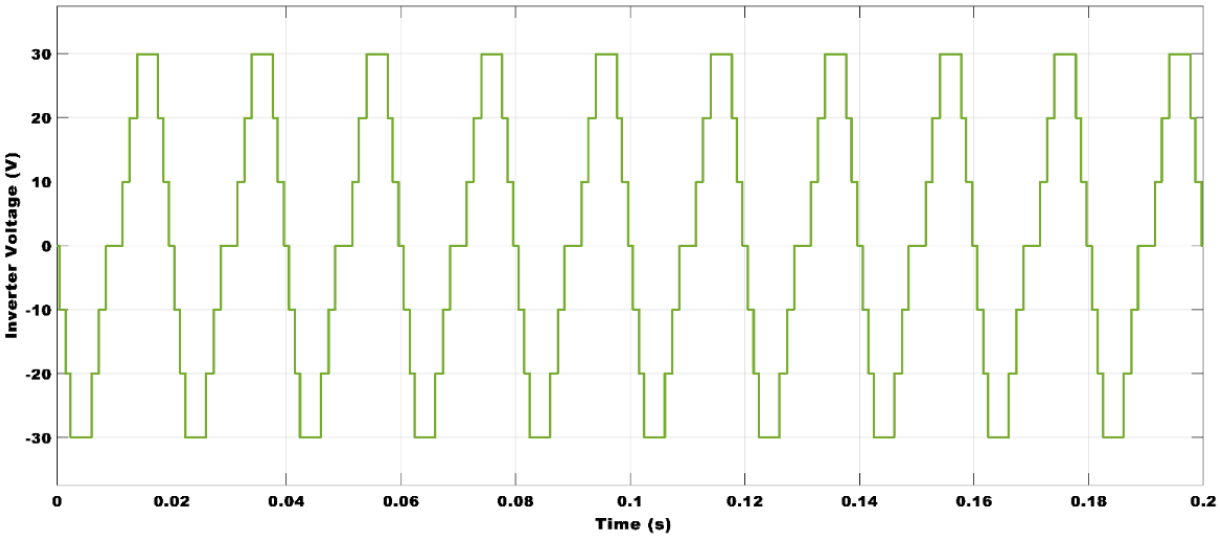

Fig. 10. The voltage waveform of a 7-level inverter.

The output voltages of the 7-level inverter are always full of harmonics as shown in Fig. 10. The table 2 presents the different values the voltage supported by each switch of the 7- level inverter.

Table 2. Switch switching table.

S1	S2	S3	S4	S5	S6	V_{an}
1	0	0	1	0	0	V_{dc}
1	0	0	0	0	1	$2V_{dc}/3$
1	0	0	0	1	0	$V_{dc}/3$
1	0	1	0	0	0	0
0	1	0	0	0	1	$-V_{dc}/3$
0	1	1	0	1	0	$-2V_{dc}/3$
0	1	0	0	0	0	$-V_{dc}$

Table 2 gives the different these values that each switch of the seven-level inverters supports.

2.2.9. Block diagram of the overall system in Simulink

Fig. 11 shows the global diagram, which consists of the PVG, converter, inverter, active filter and networks, through a PCC which is determined. It represents the block diagram realized in Simulink. It highlights the global system used: the generators connected to the choppers boosted by the MPPT control, the seven-level inverters upstream of the active multicell filters. A transformer is placed upstream of the electrical networks to act as a disconnector. The electrical networks are three-phase and balanced before the injection of the currents from the 7 level inverters.

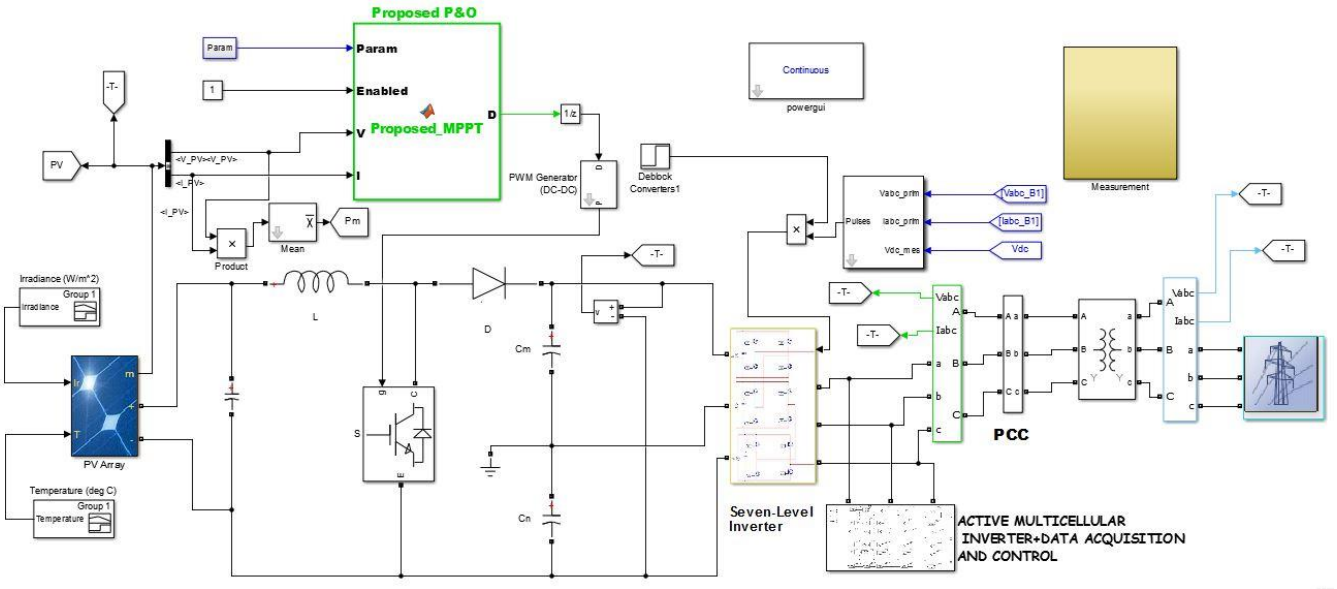

Fig. 11. Block diagram of the system.

2.2.10. Load Profile

Synchronization is required to change a two phase into a three-phase transformation which is known park transform[12].

. These voltages undergo the Park transformation known as three-phase two-phase, and are controlled and injected into the power grids utilities, through the 4-level multicellular inverter. The electrical networks constitute the load.

$$\begin{bmatrix} v_0 \\ v_\propto \\ v_\beta \end{bmatrix} = \sqrt{\frac{2}{3}} \begin{bmatrix} \frac{1}{\sqrt{2}} & \frac{1}{\sqrt{2}} & \frac{1}{\sqrt{2}} \\ 1 & \frac{1}{2} & -\frac{1}{2} \\ 0 & \frac{\sqrt{3}}{2} & -\frac{\sqrt{3}}{2} \end{bmatrix} \begin{bmatrix} v_{an} \\ v_{bn} \\ v_{cn} \end{bmatrix} \quad (9)$$

$$\begin{bmatrix} I_0 \\ I_\propto \\ I_\beta \end{bmatrix} = \sqrt{\frac{2}{3}} \begin{bmatrix} \frac{1}{\sqrt{2}} & \frac{1}{\sqrt{2}} & \frac{1}{\sqrt{2}} \\ 1 & \frac{1}{2} & -\frac{1}{2} \\ 0 & \frac{\sqrt{3}}{2} & -\frac{\sqrt{3}}{2} \end{bmatrix} \begin{bmatrix} I_{ca} \\ I_{cb} \\ I_{cc} \end{bmatrix} \quad (20)$$

The currents are broken down into the fundamental ($\bar{I}_\propto, \bar{I}_\beta$) and the harmonics ($\tilde{I}_\propto, \tilde{I}_\beta$):

equations of these transformations' models are given in equations (Eq. 2, 4 and 6.)

The reference voltages are the output voltages of the seven-level inverters

The equations that lead to Park's direct transformation [22] are below. In the space α-β voltages and currents can be expressed:

$$\begin{cases} I_\propto = \bar{I}_\propto + \tilde{I}_\propto \\ I_\beta = \bar{I}_\beta + \tilde{I}_\beta \end{cases} \quad (31)$$

The instantaneous harmonic active and reactive powers are calculated by the relation:

$$\begin{bmatrix} \tilde{p} \\ \tilde{q} \end{bmatrix} = \begin{bmatrix} v_\propto & v_\beta \\ -v_\beta & v_\propto \end{bmatrix} \quad (42)$$

To simultaneously compensate for reactive power and harmonic currents generated by the non-linear load, reference currents should include $\tilde{p}, \tilde{q}$ et $\bar{q}$ as below:

$$\begin{bmatrix}\tilde{I}_{\propto-ref}\\ \tilde{I}_{\beta-ref}\end{bmatrix}=\frac{1}{v_{\alpha}^{2}+v_{\beta}^{2}}\begin{bmatrix}v_{\propto} & -v_{\beta}\\ v_{\beta} & v_{\propto}\end{bmatrix}\begin{bmatrix}\tilde{p}\\ \tilde{q}\end{bmatrix}+\frac{1}{v_{\alpha}^{2}+v_{\beta}^{2}}\begin{bmatrix}v_{\propto} & -v_{\beta}\\ v_{\beta} & v_{\propto}\end{bmatrix}\begin{bmatrix}0\\ \bar{q}\end{bmatrix} \quad (53)$$

The reference currents in the a-b-c tag are given by:

$$\begin{bmatrix}I_{ref1}\\ I_{ref2}\\ I_{ref3}\end{bmatrix}=\sqrt{\frac{2}{3}}\begin{bmatrix}1 & 0\\ -\frac{1}{2} & \frac{\sqrt{3}}{2}\\ -\frac{1}{2} & -\frac{\sqrt{3}}{2}\end{bmatrix}\begin{bmatrix}\tilde{I}_{\propto-ref}\\ \tilde{I}_{\beta-ref}\end{bmatrix} \quad (64)$$

The model used is that of the PQ theory [23] developed and implemented in MATLAB/Simulink to extract the reference currents.

2.2.11. Simulink model of park's transformation from ABC to DQ and DQ to ABC phase.

Fig. 12 presents the block diagram model in matlab/Simulink, made from the previous equations (Eq.3,6,8) [24]:

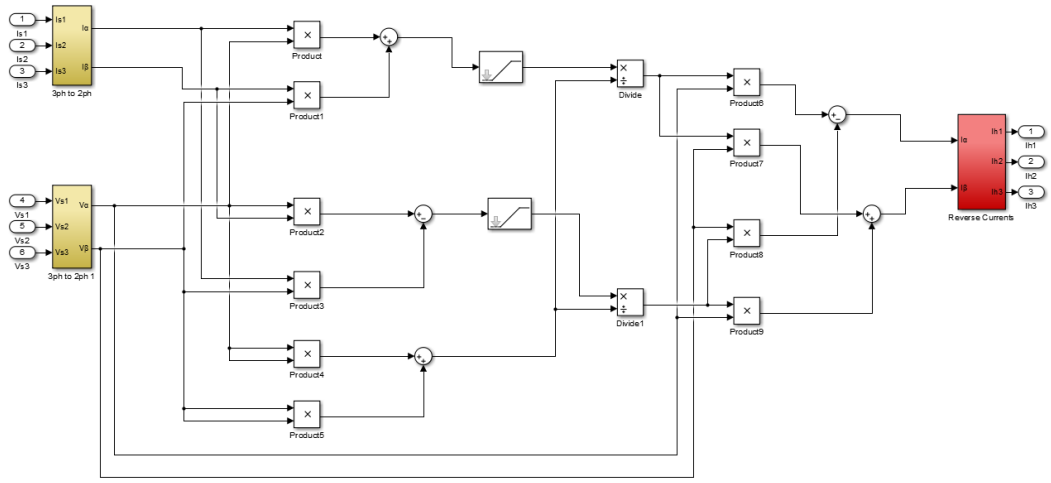

Fig. 12. The Block diagram of the park transform.

2.2.12. Identification of harmonics of Fourier transform

The Fourier transform allows to identify harmonics of even and odd rank [25]. Assuming V_{aM}, the line-to-phase voltage grid, the equations are follow:

$$V_{aM(\omega t)}=\sum_{n=1}^{\infty}(a_n(\sin(n\omega t));\ b_n=0 \quad (75)$$

$$\begin{cases}b_n=\frac{4}{\pi}\int_0^{\frac{\pi}{2}}V_{aM(\omega t)}(\sin(n\omega t)\,d(\omega t),\\ a_n=0\\ b_n=0\ \forall n\end{cases} \quad (16)$$

After integration, equations of harmonics of order n are given:

$$h_n=\frac{4V_a}{n\pi}\left(S_1cos(n\propto_1)+S_2cos(n\propto_2)+\cdots.+S_pcos(n\propto_p)\right) \quad (87)$$

For the given order i harmonic we have the equations:

$$h_1=\frac{4V_a}{\pi}\left(S_1cos(\propto_1)+S_2cos(\propto_2)+\cdots.+S_pcos(\propto_p)\right)\ n=1 \quad (98)$$

$$h_i=\frac{4V_a}{i\pi}\left(S_1cos(i\propto_1)+S_2cos(i\propto_2)+\cdots.+S_pcos(i\propto_p)\right)\ n=i \quad (109)$$

Where:

n : Odd number
V_a : Supply voltage or $V_a = V_b = V_c$, resulting from the inverse transformation of Park
h_1 : Fundamental of the output voltages
$\propto_i$: Switching angles
S_i : sign of cos

$$0 < \propto_2 < \propto_3 \ldots . < \propto_p < \frac{\pi}{2}$$

$$THD = \frac{\sqrt{\frac{x^2x^2}{8} - \frac{\pi}{4}\sum_{i=0}^{p-1}(2i+1)\alpha_{i+1} - \left(\sum_{i=1}^{p} cos(\alpha_i)\right)^2}}{\sum_{i=1}^{p} cos(\alpha_i)} \quad (20)$$

The THD is defined as follow [26]:

$$THD(\%) = 100 * \sqrt{\sum_{i=2}^{n=\infty}\left(\frac{{I_h}^2}{{I_1}^2}\right)} \quad (21)$$

Where:

I_h : harmonic component of rank h

I_1: : fundamental component

3. Results and discussion

3.1. Current waveform

3.1.1. current Output before filtering

The presence of harmonics in electrical networks distorts the currents, as shown in Fig.13. The role of multicell filters is to remove these disturbing lines as shown in the Fig. 17.

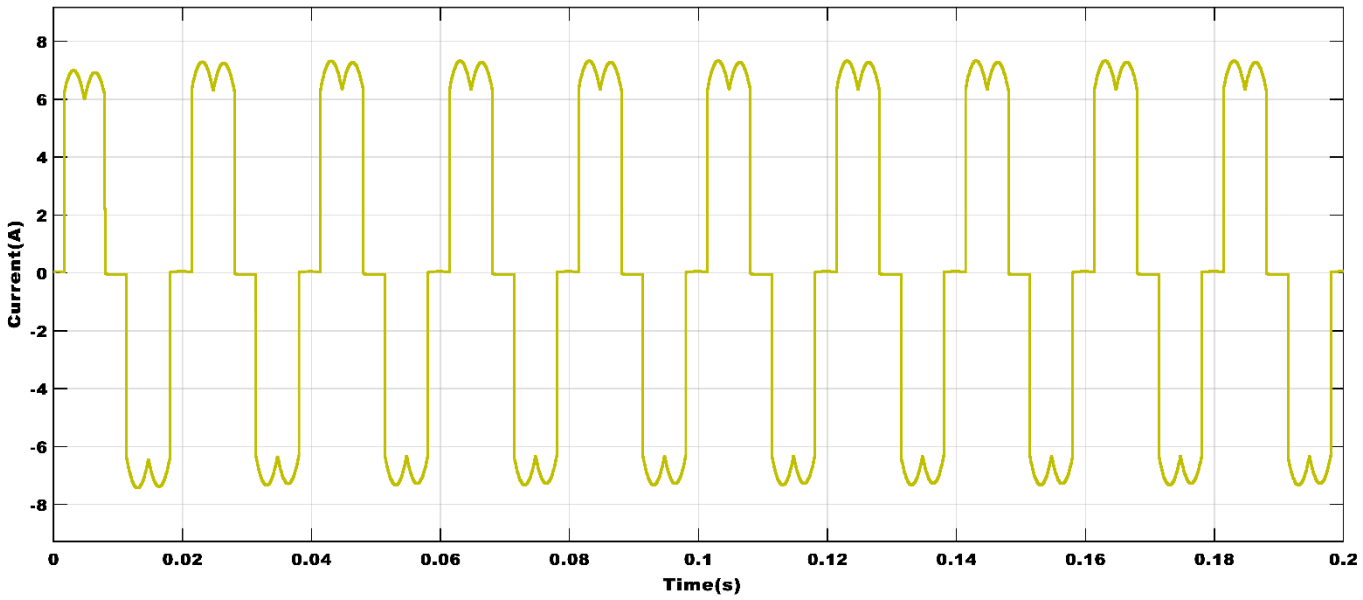

Fig. 13. Current waveform before filtering.

3.1.2. Current injected by the filter in the network

Fig. 14, shows the shape of the currents that the active filters inject in the networks, in order to cancel the signals whose frequencies are odd multiples of 50 Hertz. In this work, the active filter eliminates the harmonic lines up to order 21. However, the most harmful harmonics are those with a rank lower than or equal to 21.

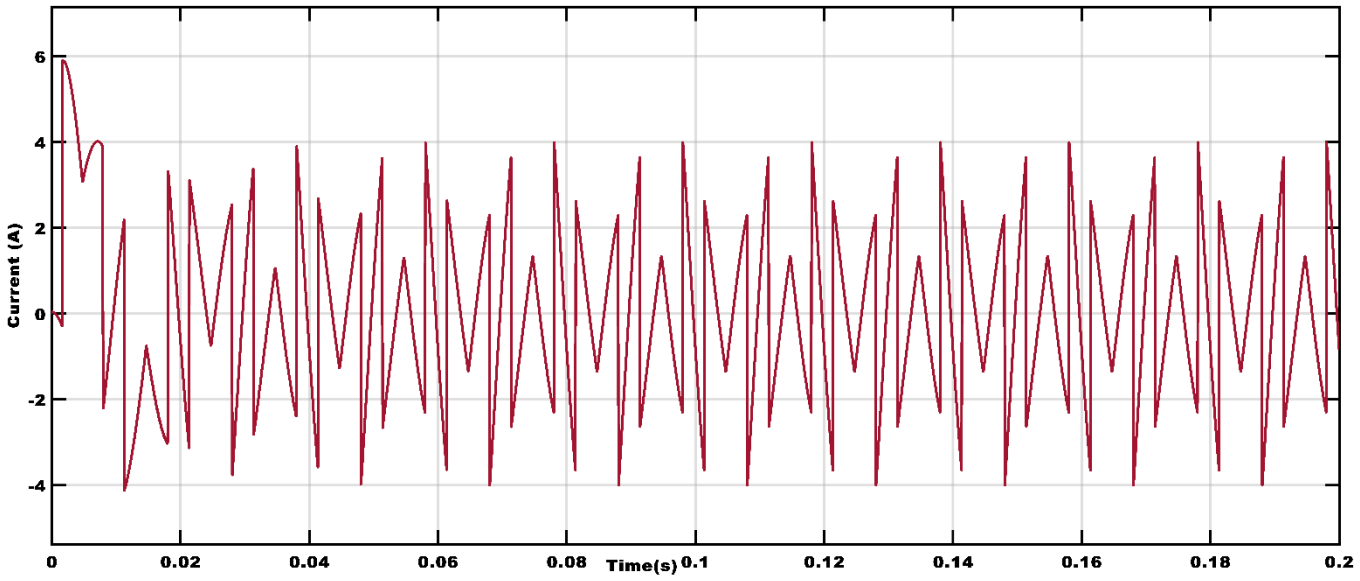

Fig. 14. Reference current of the filter to be injected in the Network.

3.1.3. Module under partial shading

Considering one module protected by two diodes under PSC of one cell by 75%, and the of this module and the simulation of the performance using both the classic and the improved P&O methods are both simulated as shown in Fig. 15.

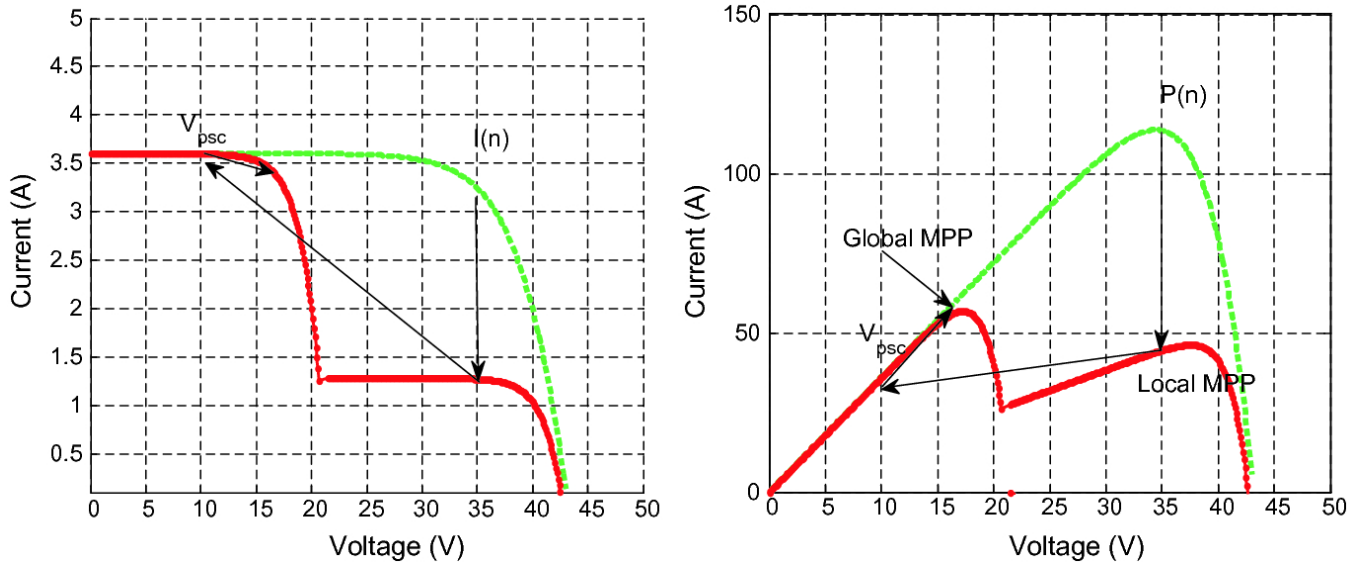

Fig. 15. I–V and P–V characteristics for improved P&O MPPT algorithm under partial shading.

Fig.16. shows the MPP when implementing both classical algorithm and improved P&O algorithms, comparing them with the theoretically calculated MPP. It is noted that the tracking efficiency increased drastically from 88% with classic P&O to 99% with improved P&O under steady-state condition for some variations.

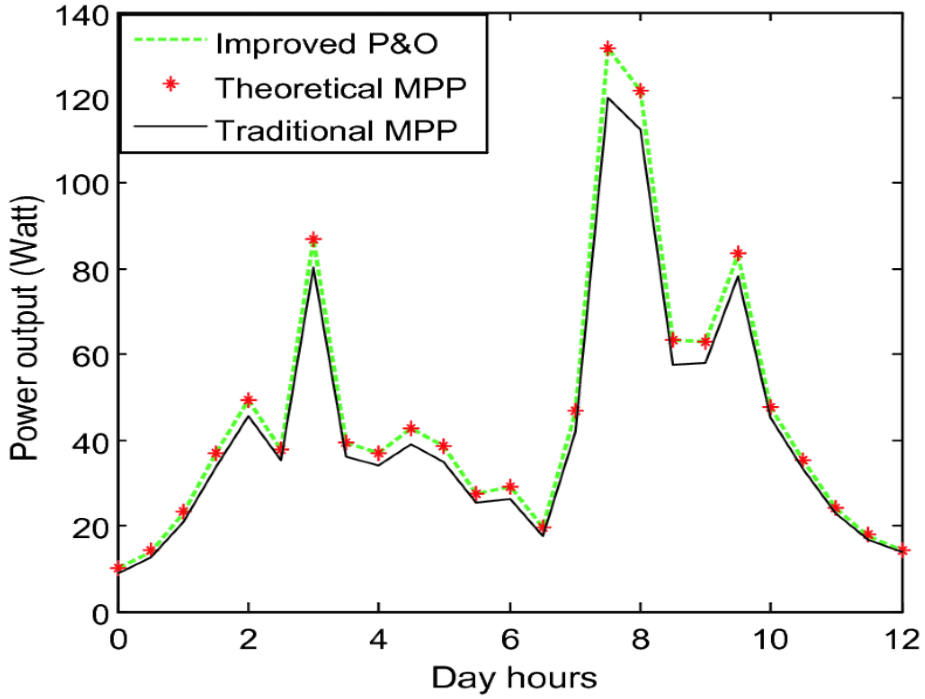

Fig. 16. Power generated by the MPP algorithm

Fig. 17 shows clearly the harmonics of odd order that are eliminated, up to the rank n=21. It is shown by the disappearance of their spectrum. However, the most harmful harmonics are those of odd rank and especially of rank 3, 5, 7,9 [27]. In the same way as it is found in the literature review, [28] in their work obtains a low THD, by inserting a transformer in the system configuration. To reduce the harmonics [3] used to realize an active filter based on multilevel inverters, and thus the increase of the irradiance would reduce the THD. [29] realized that it is possible to eliminate these harmonic lines by hybridization of several renewable sources, which still leaves limitations that [13] show in their work. On the other hands, [30] from two secondary sources have found an acceptable rate for ranks less than 9. But from all these works, nothing guarantees that the values would be maintained if the rate of harmonics is calculated until rank 21.

3.1.4. Total Harmonic Distortion (THD)

The THD of the current of the inverter provides a very low rate, for a fundamental from 65 to 50Hz. Harmonic lines have almost disappeared as shown in Fig. 17.

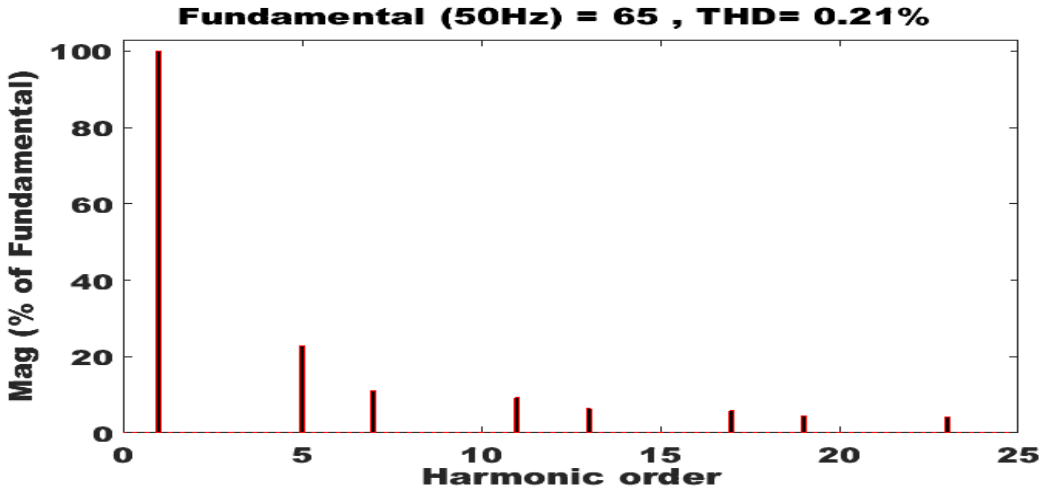

Fig. 17. Frequency spectrum of the current after filtering.

The voltage and current of the inverter are in phase, Fig. 18 which proves the power factor correction and the balance of the network after increasing the voltages of the seven-stage inverters. Our proposed model is interesting because we have reduced the THD with a reduced number of switches that most often create losses, thanks to the MPPT algorithm improved on the Fig. 4.

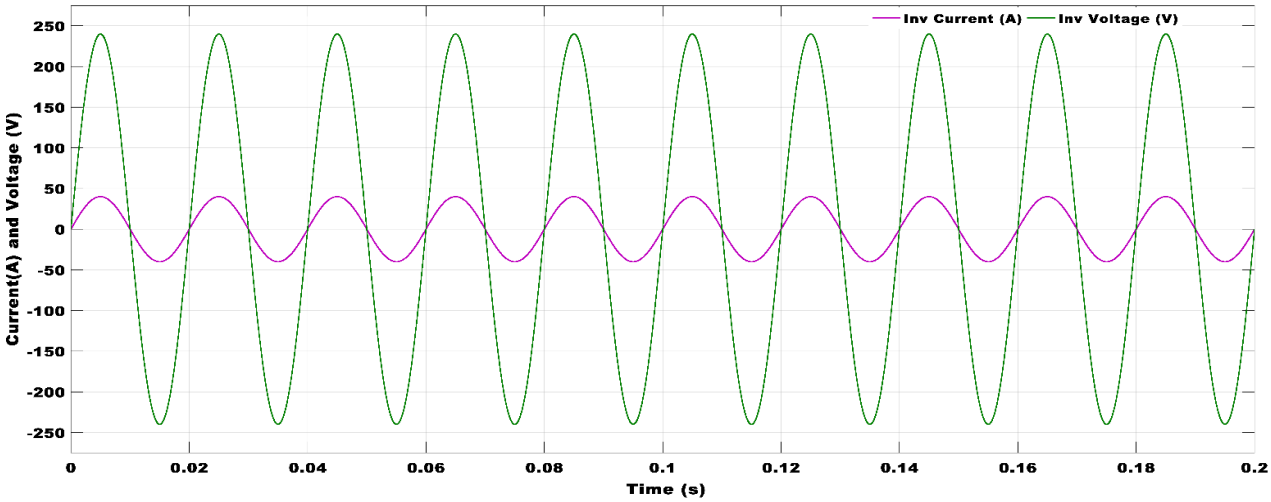

Fig. 18. Current and voltage wave forms of the 7-level inverter after filtering.

4. Conclusion

In this work, the modeling of the step-up converter and the four multi-cell filters with three switching cells per arm have been made, the 7-level inverter is presented. The analysis of the performance of the filter and the improved algorithm is widely commented on. This filtering system is an ideal solution to solve the problem of load shedding in isolated sites as in connected networks for optimal control of reactive power through a digital data acquisition card. The input voltage of the filter is dimensioned so as to allow control by multiple agents; which gives a perspective to smart grids. The voltage and current of each phase of the three-phase seven-level inverter show the correction of the power factor after injecting the photovoltaic energy into the power grids. In this sense, the MPPT algorithm has proven its performance, while multicellular filters have confirmed their great interest. The value of the THD found is much lower than that allowed by the regulations on distributed generation. In addition, this system is designed to be applied in intelligent networks with the possibility of having an efficient control by multi-agents of the real-time data. And finally, the battery bank can be placed at the common coupling point for the purpose of serving isolated sites.

List of abbreviations

THD	:	Total Harmonic Distortion
MPPT	:	Maximum Power Point Tracking
PVG	:	Photovoltaic Generators
IEEE	:	Institute of Electrical and Electronics Engineers
P&O	:	Perturb and observe
PWM	:	Pulse width modulation
PLL	:	Phase-Locked Loop

Declaration of competing interest

The authors declare that they have no known competing financial interests or personal relationships that could have appeared to influence the work reported in this paper.

References

[1] Špelko A, Blažič B, Papič I, Herman L. Active Filter Reference Calculations Based on Customers' Current Harmonic Emissions. Energies 2021;14:220. https://doi.org/10.3390/en14010220.

[2] Chawla P, Lalwani M. Analysis and simulation of reactive power theory for harmonic elimination using shunt active power filter. Int J Intell Sustain Comput 2021;1:181. https://doi.org/10.1504/ijisc.2021.113322.

[3] Xiong L, Nour M, Radwan E. Harmonic analysis of photovoltaic generation in distribution network and design of adaptive filter. Int J Comput Digit Syst 2020;9:77–85. https://doi.org/10.12785/ijcds/090108.

[4] Lazarte JC, Vasios O, Meliopoulos A. Analysis of the operation and power quality of a microgrid with photovoltaic sources. 2018 North Am. Power Symp. NAPS 2018, Institute of Electrical and Electronics Engineers Inc.; 2019. https://doi.org/10.1109/NAPS.2018.8600568.

[5] Wu H, Wang X. A Mode-Adaptive Power-Angle Control Method for Transient Stability Enhancement of Virtual Synchronous Generators. IEEE J Emerg Sel Top Power Electron 2020;8:1034–49. https://doi.org/10.1109/JESTPE.2020.2976791.

[6] Husen AY, Younis KH, Fatah AA. High Harmonic Reduction Using Passive Filters of Mountain Steel Company. Zanco J Pure Appl Sci 2021;33. https://doi.org/10.21271/zjpas.33.1.19.

[7] Liao S, Huang M, Zha X, Guerrero JM. Emulation of Multi-Inverter Integrated Weak Grid Via Interaction-Preserved Aggregation. IEEE J Emerg Sel Top Power Electron 2020:1–1. https://doi.org/10.1109/jestpe.2020.2988364.

[8] Amorim WCS, Mendonca DDC, Callegari JMS, Silva MP, Pereira

HA, Cupertino AF. Comparison of current grid controllers in a DG inverter with grid harmonic distortion. 2018 13th IEEE Int. Conf. Ind. Appl. INDUSCON 2018 - Proc., 2019. https://doi.org/10.1109/INDUSCON.2018.8627162.

[9] Tang CY, Chen YF, Chen YM, Chang YR. DC-Link Voltage Control Strategy for Three-Phase Back-to-Back Active Power Conditioners. IEEE Trans Ind Electron 2015;62:6306–16. https://doi.org/10.1109/TIE.2015.2420671.

[10] Kavya M, Jayalalitha S. A novel coarse and fine control algorithm to improve Maximum Power Point Tracking (MPPT) efficiency in photovoltaic system. ISA Trans 2021. https://doi.org/10.1016/j.isatra.2021.03.036.

[11] Ali K, Khan L, Khan Q, Ullah S, Ali N. Neurofuzzy robust backstepping based MPPT control for photovoltaic system. Turkish J Electr Eng Comput Sci 2021;29:421–36. https://doi.org/10.3906/ELK-1907-15.

[12] Pigazo A, Moreno VM, Estébanez EJ. A recursive park transformation to improve the performance of synchronous reference frame controllers in shunt active power filters. IEEE Trans Power Electron 2009;24:2065–75. https://doi.org/10.1109/TPEL.2009.2025335.

[13] Heru Pratomo L. A new topology of a single-phase five-level inverter. Indones J Electr Eng Informatics 2020;8:447–56. https://doi.org/10.11591/ijeei.v8i3.1766.

[14] Mahmood A, Zaid M, Ahmad J, Khan MA, Khan S, Sifat Z, et al. A Non-Inverting High Gain DC-DC Converter with Continuous Input Current. IEEE Access 2021;9:54710–21. https://doi.org/10.1109/ACCESS.2021.3070554.

[15] Nabipour M, Razaz M, Seifossadat SG, Mortazavi SS. A new MPPT scheme based on a novel fuzzy approach. Renew Sustain Energy Rev 2017;74:1147–69. https://doi.org/10.1016/j.rser.2017.02.054.

[16] Pérez Archila LM, Bastidas Rodríguez JD, Correa R. Implicit modelling of series-parallel photovoltaic arrays using double-diode model and its solution. Sol Energy 2021;214. https://doi.org/10.1016/j.solener.2020.11.036.

[17] Nabae A, Takahashi I, Akagi H. A new neutral-point-clamped PWM inverter. IEEE Trans Ind Appl 1981;IA-17:518–23. https://doi.org/10.1109/TIA.1981.4503992.

[18] Rivera S, Kouro S, Wu B, Leon JI, Rodríguez J, Franquelo LG. Cascaded H-bridge multilevel converter multistring topology for large scale photovoltaic systems. IEEE Int. Symp. Ind. Electron., Gdansk, Poland: IEEE; 2011, p. 1837–44. https://doi.org/10.1109/ISIE.2011.5984437.

[19] Brambilla A, Gambarara M, Garutti A, Ronchi F. New approach to photovoltaic arrays maximum power point tracking. 30th Annu. IEEE Power Electron. Spec. Conf., IEEE; 1999, p. 632–7 vol.2. https://doi.org/10.1109/PESC.1999.785575.

[20] Hassaine L, Olías E, Haddadi M, Malek A. Asymmetric SPWM used in inverter grid connected,. J Renew Energies 2007;10:421–9.

[21] Rajeswari R. power quality improvement of novel PWM based 15 level inverter for modified unified power quality conditioner (UPQC) 2015.

[22] zhao J, Huang M, Zha X. Nonlinear Analysis of PLL Damping Characteristics in Weak-Grid-Tied Inverters. IEEE Trans Circuits Syst II Express Briefs 2020;67:2752–6. https://doi.org/10.1109/TCSII.2020.2978026.

[23] Fujita H, Akagi H. A Practical Approach to Harmonic Compensation in Power Systems Series Connection of Passive and Active Filters. IEEE Trans Ind Appl 1991;27:1020–5. https://doi.org/10.1109/28.108451.

[24] Changqing C, Wang L, Guohui Y. A three-phase active power filter based on PARK transformation. Proc. 2009 4th Int. Conf. Comput. Sci. Educ. ICCSE 2009, 2009. https://doi.org/10.1109/ICCSE.2009.5228469.

[25] Grivet J-P. Chapitre 9 Analyse spectrale, transformation de Fourier numérique. In: Les Ulis, editor. Méthodes numériques appliquées, EDP Sciences; 2021, p. 183–204.

[26] Zhang X, Wu X, Tan G, Zhang W, Wang Q. A Dual-vector Model Predictive Control Method With Minimum Current THD. IEEE Trans Power Electron 2021. https://doi.org/10.1109/TPEL.2021.3065009.

[27] Senthilnathan N, Manigandan T. A novel control strategy for line harmonic reduction using three phase shunt active filter with balanced and unbalanced supply. Eur J Sci Res 2012;67.

[28] Barbu V, Chicco G, Corona F, Golovanov N, Spertino F. Impact of a photovoltaic plant connected to the mv network on harmonic distortion: An experimental assessment. UPB Sci Bull Ser C Electr Eng 2013;75.

[29] Zhang L, Sun K, Xing Y, Feng L, Ge H. A modular grid-connected photovoltaic generation system based on DC bus. IEEE Trans Power Electron 2011;26. https://doi.org/10.1109/TPEL.2010.2064337.

[30] Subudhi U, Dash S. Detection and classification of power quality disturbances using GWO ELM. J Ind Inf Integr 2021;22. https://doi.org/10.1016/j.jii.2021.100204.